

SMC/97/06

hep-ex/9704005

March, 1997

SPIN STRUCTURE FUNCTIONS

G.K. MALLOT

*Institut für Kernphysik der Universität Mainz, Becherweg 45,
D-55099 Mainz, Germany*

The experimental status of the spin-dependent structure functions as obtained from the deep inelastic scattering experiments at CERN, SLAC, and DESY is reviewed. All data show a violation of the Ellis–Jaffe sum rule. The Bjorken sum rule is found to be valid and is tested to the 10 % level.

Invited plenary talks given at the

XVI International Conference on Physics in Collision, PIC96
Mexico City, Mexico, 19–21 June, 1996

and

12th International Symposium on High-Energy Spin Physics, SPIN96
Amsterdam, The Netherlands, 10–14 September 1996

to be published in the proceedings^a

^aTo the SPIN96 proceedings a shorter version of this paper was submitted.

SPIN STRUCTURE FUNCTIONS

G.K. MALLOT

*Institut für Kernphysik der Universität Mainz, Becherweg 45,
D-55099 Mainz, Germany
email: Gerhard.Mallot@cern.ch*

The experimental status of the spin-dependent structure functions as obtained from the deep inelastic scattering experiments at CERN, SLAC, and DESY is reviewed. All data show a violation of the Ellis–Jaffe sum rule. The Bjorken sum rule is found to be valid and is tested to the 10 % level.

1 Introduction

After the discovery by the EMC^{1,2} that the contribution of the quark spins to the proton spin is much smaller than expected, new experiments were proposed and set up to study this “spin puzzle”. First was the experiment of the Spin Muon Collaboration (SMC) at CERN^{3,4,5,6,7,8} followed by the SLAC experiments^{9,10,11,12,13} and the HERMES experiment¹⁴ at DESY. In parallel intensive work started on the theoretical side. The information obtained from the measurements is twofold. On one hand the test of the Bjorken sum rule¹⁵ provides a sensitive test of QCD, on the other hand the nonperturbative spin-flavour structure of the nucleon is contained in the polarised parton distribution functions. The structure function data are by now precise enough to perform sensible QCD analyses and to determine the parton distribution functions. However, the precision of the data is still far from the quality of the spin-averaged structure function measurements and several constraints are needed in the QCD analyses. An important aim is to understand the nucleon’s spin in terms of the spins of quarks and gluons, $\Delta\Sigma = \Delta u + \Delta d + \Delta s$ and Δg , and their orbital angular momenta, L_q and L_g ,

$$\frac{1}{2} = \frac{1}{2}\Delta\Sigma + L_q + \Delta g + L_g. \quad (1)$$

It is well known from both, experiment and theory, that at high Q^2 about half of the nucleon’s longitudinal momentum is carried by the gluons. Recently, it was predicted¹⁶ that the same sharing should apply for the total angular momentum. In the Quark Parton Model the quark polarisations,

$$\Delta q = (q^+ - q^-) + (\bar{q}^+ - \bar{q}^-), \quad (2)$$

are related to the spin-dependent structure function g_1 by

$$g_1(x, Q^2) = \frac{1}{2} \sum_f e_f^2 \Delta q_f(x, Q^2), \quad (3)$$

where f runs over the quark flavours and e_f are the electrical quark charges. The notations $q^{+(-)}$ refer to parallel (antiparallel) orientation of the quark and nucleon spins.

Experimentally the spin-dependent structure functions, g_1 and g_2 , are obtained from the measured event-number asymmetries, $A_{\parallel}^{\text{raw}}$, for longitudinal orientation of the target and lepton spins, and A_{\perp}^{raw} for transverse target polarisations. These raw asymmetries range for the proton typically from a few per cent at large x to a few parts per thousand at small x . In the lepton-nucleon asymmetries, A_{\parallel} and A_{\perp} , the uncertainties of the raw asymmetries get amplified by the factor $1/P_b P_t f$ accounting for the incomplete beam and target polarisations, P_b and P_t , and the dilution factor, f . Typical target materials contain a large fraction of unpolarisable nucleons and f denotes the fraction of the total spin-averaged cross section arising from the polarisable nucleons. For the target materials used, f varies from about 0.13 (butanol), over 0.17 (ammonia) to 0.3 (^3He). For deuterated butanol and ammonia f is 0.23 and 0.3, respectively, while for the proton and deuteron gas targets of the HERMES experiment f is close to unity. The neutron structure functions are either obtained from the combination of proton and deuteron data or from experiments using ^3He targets. The deuteron asymmetries are slightly reduced from the average of proton and neutron asymmetries due to the D-state component in the deuteron wave function. The ^3He asymmetry is mainly due to the unpaired neutron, however a small proton contribution has to be corrected for. Due to the cancellation of the isotriplet part in g_1^d the measurements using deuteron targets are most sensitive to the flavour-singlet part, $\Delta\Sigma$, and thus to the violation of the Ellis–Jaffe sum rule. The structure functions, g_1 and g_2 , are related to the virtual photon asymmetries, A_1 and A_2 , via

$$A_{\parallel} = D(A_1 + \eta A_2), \quad A_{\perp} = d(A_2 - \xi A_1), \quad (4)$$

$$A_1 = \frac{g_1 - \gamma^2 g_2}{F_1}, \quad A_2 = \gamma \frac{g_1 + g_2}{F_1}. \quad (5)$$

Here $F_1 = F_2(1 + \gamma^2)/2x(1 + R)$ is the well-known spin-averaged structure function and $\gamma^2 = Q^2/\nu^2$, η , and ξ are kinematic factors, which are small in most of the kinematic domain covered by the data. The variables ν and $Q^2 = -q^2$ denote respectively the energy transfer and negative square of the 4-momentum transfer. The kinematic factors, D and d , account for the incomplete transverse polarisation of the virtual photon. With longitudinal target

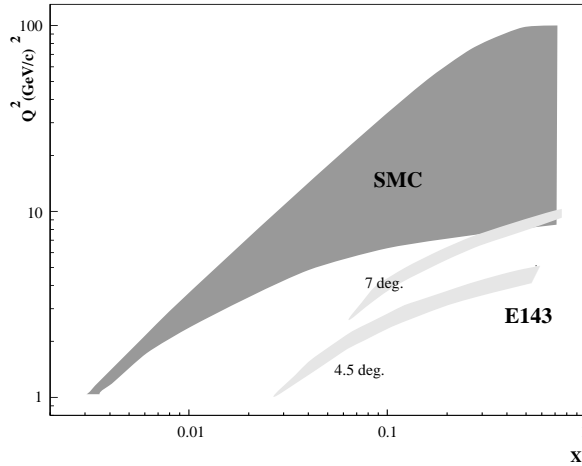


Figure 1: The kinematic ranges covered by the SMC and E-143 experiments.

polarisation predominantly g_1 is determined, while experiments with transverse target polarisation are sensitive to $g_1 + g_2$. The virtual photon asymmetries are bounded by $|A_1| \leq 1$ and $|A_2| \leq \sqrt{R}$, where $R = \sigma_L/\sigma_T$ is the longitudinal-to-transverse photoabsorption cross-section ratio known, like F_2 , from unpolarised deep inelastic scattering.

2 The Experiments

New data from the 1995 runs come from the SMC⁷ (deuteron), the HERMES experiment¹⁴ (^3He) and the SLAC experiment E-154¹³ (^3He , preliminary). Some important parameters of these and the earlier experiments are summarised in Table 1 and the kinematic ranges of the SMC and E-143 experiments are compared in Fig. 1.

The experiments of the SMC were performed at the CERN muon beam at 190 GeV using a large, double-cell solid-state polarised target. Data with parallel and antiparallel orientation of the lepton and target spins were taken simultaneously. This technique cancels most systematic uncertainties and overcomes the problem that the natural polarisation of the muon beam cannot effectively be reversed. Average polarisations of 86 % and 50 % were achieved for the butanol and deuterated butanol targets used in the years 1992–1995. The opposite polarisation of the material in the two 65 cm long cells was reversed

Table 1: Parameters of the experiments

Experiment	Lab.	Beam		$\langle Q^2 \rangle$ [GeV ²]	x range	Targets
E-80/130	SLAC	22 GeV	e	4	0.18 $\leq x \leq 0.7$	p
EMC	CERN	200 GeV	μ	10.7	0.01 $\leq x \leq 0.7$	p
SMC	CERN	190 GeV	μ	10	0.003 $\leq x \leq 0.7$	p, d
E-142/143	SLAC	29 GeV	e	2-3	0.03 $\leq x \leq 0.8$	³ He, p, d
E-154/155	SLAC	48 GeV	e	5	0.014 $\leq x \leq 0.7$	³ He, p, d
HERMES	DESY	27 GeV	e	3	0.023 $\leq x \leq 0.6$	³ He, p, d

every 5 h. In the 1996 run a proton target made of ammonia was employed. The incoming and scattered muons were analysed by magnetic spectrometers. Hadrons produced in the scattering were also detected. However, a particle identification beyond electron-hadron separation was not attempted. A dedicated spectrometer downstream of the main scattering spectrometer measures the about 80 % polarisation of the muon beam by two methods. One is based on the dependence of the energy spectrum of the decay positrons on the parent muon polarisation, the other uses the asymmetry in polarised muon-electron scattering from a magnetised iron foil. The domain unique to the SMC experiment is high Q^2 and small x which is essential for the extrapolations to $x \rightarrow 0$ and for QCD analyses of the structure function data.

The SLAC experiments E-142/E-143 and E-154 were performed at the SLAC electron beam in End Station A with energies up to 29 and 48 GeV, respectively. The rather low energy of the incoming electron limits the accessible kinematic range. Apart from the E-142 experiment (39 %) electron polarisations of 80 % were reached using strained-lattice GaAs photocathodes. The electron polarisation was varied randomly on a pulse-by-pulse basis and measured by Moller scattering from thin ferromagnetic foils. For the neutron experiments, E-142 and E-154, a ³He gas target with a pressure of 10 bar was used and polarisations of 30-40 % were reached by spin-exchange with optically pumped rubidium vapour. With the ammonia targets used in the E-143 experiment and foreseen for the E-155 experiment polarisations of 65-80 % for NH₃ and 25 % for ND₃ were reached. For the E-155 experiment running in 1997 also a ⁶LiD deuteron target is foreseen. The lithium-6 nucleus can be understood as an α +d system,¹⁷ yielding for ⁶LiD a favourable dilution factor of $f = 0.5$. The scattered electrons were analysed by two magnetic spectrometers placed under different scattering angles to increase the acceptance. With the intense electron beams much higher luminosities than with muon beams

can be achieved yielding smaller statistical errors. The accuracy of the first moments obtained from the SLAC experiments is thus systematics limited.

A different technique is applied in the HERMES experiment which started data-taking in 1995. The electrons in the HERA ring self-polarise by the Sokolov–Ternov effect to about 50 %. Spin rotators before and after the target provide longitudinal electron polarisation. A 40 cm long windowless storage cell placed in the ring is filled with up to 10^{17} atoms/s which are then pumped away at both ends of the cell. Thus pure polarised proton, deuteron, and ^3He targets can be used without diluting the asymmetries by the presence of unpolarised target materials. This target technique is in particular ideal to study hadrons produced in the deep inelastic scattering process. The polarisation of the hydrogen and the deuterium target can be changed within milliseconds while obtaining equilibrium in the ^3He target takes about 20 s. With the ^3He target employed in the 1995 run polarisations of 50 % were reached. The scattered electrons are analysed in an open magnetic spectrometer. Particle identification is provided by the combined information from a TRD, a threshold Cherenkov counter, and a lead-glass calorimeter. Due to the limited energy of the HERA electron ring of 27 GeV HERMES cannot extend the kinematic range of the SMC and SLAC experiments. However, it will provide high-precision semi-inclusive data.

3 Asymmetries and Structure Functions

The virtual-photon asymmetries measured by the various experiments with proton, deuteron, and neutron targets are summarised for $Q^2 > 1 \text{ GeV}^2$ in Fig. 2. Although the SMC data were taken at an about six-times higher value of Q^2 than the SLAC E-143 data the agreement between the two data sets is excellent. Thus, in the region of overlap, the data are compatible with no Q^2 dependence of A_1 . Asymmetries for $Q^2 < 1 \text{ GeV}^2$ were published by the E-143 Collaboration¹⁸ and the SMC.^{8,7} However, due to higher-twist contributions they are difficult to interpret. From the asymmetries and Eqs. 5 the structure function g_1 is obtained as

$$g_1(x, Q^2) = \frac{F_2(x, Q^2)}{2x(1 + R(x, Q^2))} (A_1(x, Q^2) + \gamma A_2(x, Q^2)). \quad (6)$$

Usually the term γA_2 is neglected, what is consistent with experimental results for A_2 .^{8,7,12} In the analysis of some SLAC experiments, where γ^2 is larger than in the high-energy muon experiments, Eqs. 4 were solved for both, A_1 and A_2 . In all analyses the parametrisations of F_2 by the NMC^{19,20} and of R by SLAC²¹ were used. New R data from the NMC²² for $x < 0.1$ agree

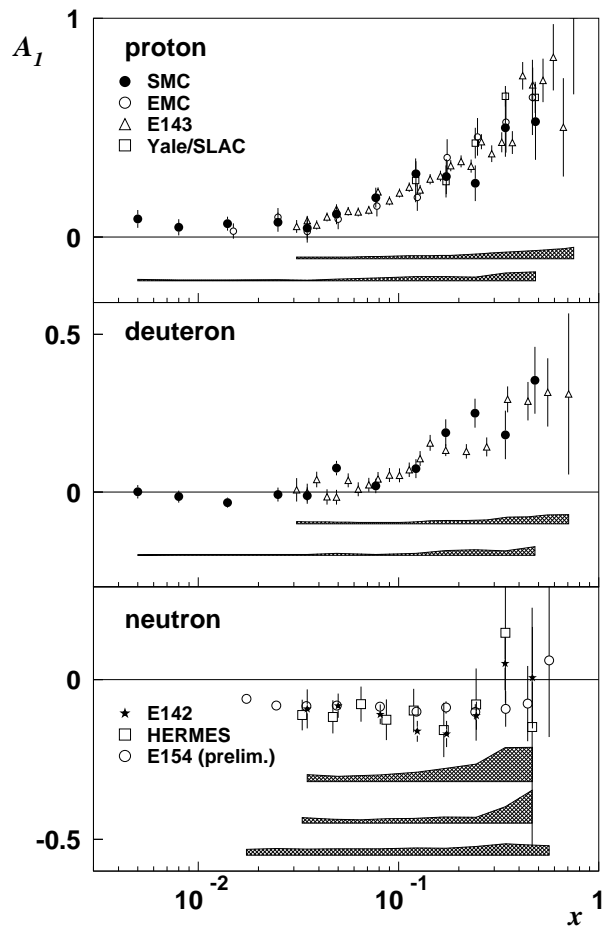


Figure 2: The virtual-photon asymmetry, A_1 , as a function of x . The shaded bands indicate the systematic errors, from top to bottom: proton: E-143, SMC; deuteron: E-143, SMC; neutron: E-142, Hermes, E-154.

well with R_{QCD} , where R_{QCD} is calculated²³ in perturbative QCD using the experimental gluon distribution function. In this x region, previously basically uncovered by experiments, the SLAC R parametrisation deviates somewhat from the data. Note that apart from radiative corrections and Q^2 extrapolations the R dependence cancels in the experimental g_1 , when the same values of R were used in the g_1 and F_2 analyses. For a recent review of the unpo-

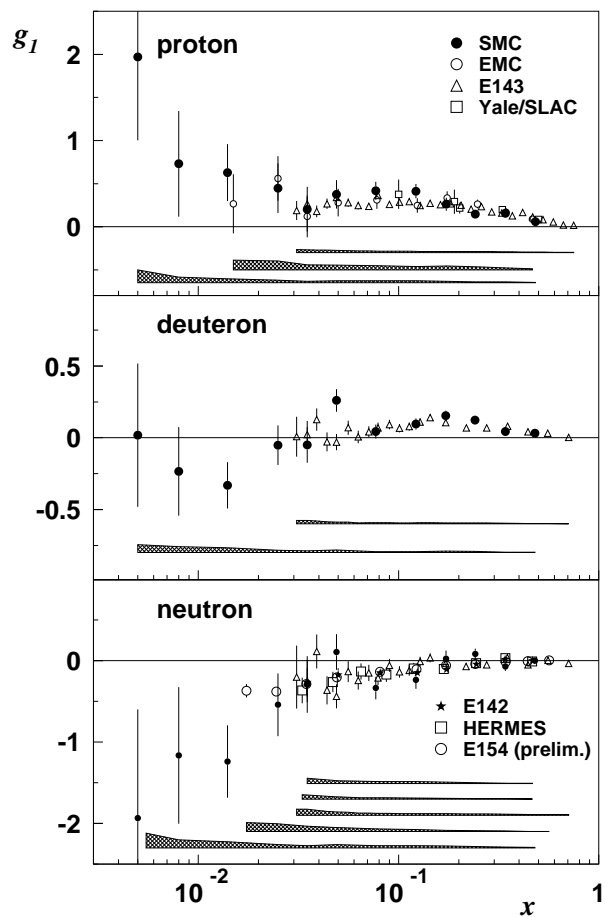


Figure 3: The structure function $g_1(x, Q^2)$ as a function of x at the Q^2 of the individual measurements. The systematic errors are indicated by the shaded bands, from top to bottom: proton: E-143, EMC, SMC; deuteron: E-143, SMC; neutron: E-142, Hermes, E-143, E-154, SMC. The E-143 and SMC neutron data are calculated from the proton and deuteron data.

larised structure functions with emphasis on the fixed-target experiments see Ref. [24].

The structure function data at the Q^2 of the individual measurements are shown in Fig. 3. The values of Q^2 vary from about 1 GeV^2 for the smallest- x point of each data set to typically 50 GeV^2 (10 GeV^2) for the largest- x point

of the SMC (SLAC) data. A study of the Q^2 dependence of A_1 using the combined SMC/EMC and SLAC data was first published¹⁸ by the E-143 Collaboration. No significant Q^2 dependence was found for $Q^2 > 1 \text{ GeV}^2$. For this analysis only one SMC data point per x -bin at an average Q^2 was available. A compilation of all now available deuteron asymmetries (SMC/E-143) is shown in Fig. 4. The proton data are in precision and kinematic coverage similar to the deuteron data. Still the experimental precision is not sufficient to reveal any Q^2 dependence of A_1 . It has to be noted that in the small- x region, where rather large effects are expected, the lever arm in Q^2 is very limited.

With more precise data available in a large kinematic range and after the next-to-leading order splitting functions were calculated^{25,26} in 1995 QCD analyses of the g_1 data start to become sensible.^{27,28,29,30} From these analyses the size of the Q^2 dependence of g_1 can be estimated. Using the method and code of Ref. [29] the SMC repeated⁸ the QCD analysis using all EMC/SMC/E-143 proton and deuteron data (Fig. 5). Although the neutron data were not included in the fit, the agreement is excellent (Fig. 6). A study of the systematic uncertainties showed that the main error sources are the choice of the factorisation and renormalisation scales, the parametrisations of the parton distribution functions, and the uncertainty in the strong coupling constant. Due to these uncertainties the predicted Q^2 dependence in a given x bin can vary considerably, in particular in the small- x region where the Q^2 slope of g_1 changes sign. The systematic errors were accounted for in the evaluation of the sum rules by the SMC. A similar study including also the E-142 and the preliminary E-154 neutron data was performed³⁰ by the authors of the evolution code with similar results.

The data for the asymmetry A_2^p and A_2^d from the SMC^{4,8,7} and the E-143 Collaboration¹² are compatible with zero in the whole covered x range with a possible exception of A_2^p for $x > 0.2$ (Fig. 7). The resulting structure functions, $g_2^{p,d}$, are shown for the SLAC data in Fig. 8. The solid line in Fig. 8 represents the twist-2 part,³¹ g_2^{ww} , which is calculable from g_1 ,

$$g_2^{\text{ww}}(x, Q^2) = -g_1(x, Q^2) + \int_x^1 \frac{g_1(y, Q^2)}{y} dy. \quad (7)$$

The data agree well with g_2^{ww} and a possible twist-3 contribution, which relates to quark-gluon correlations,³² cannot be resolved within the accuracy of the present data.

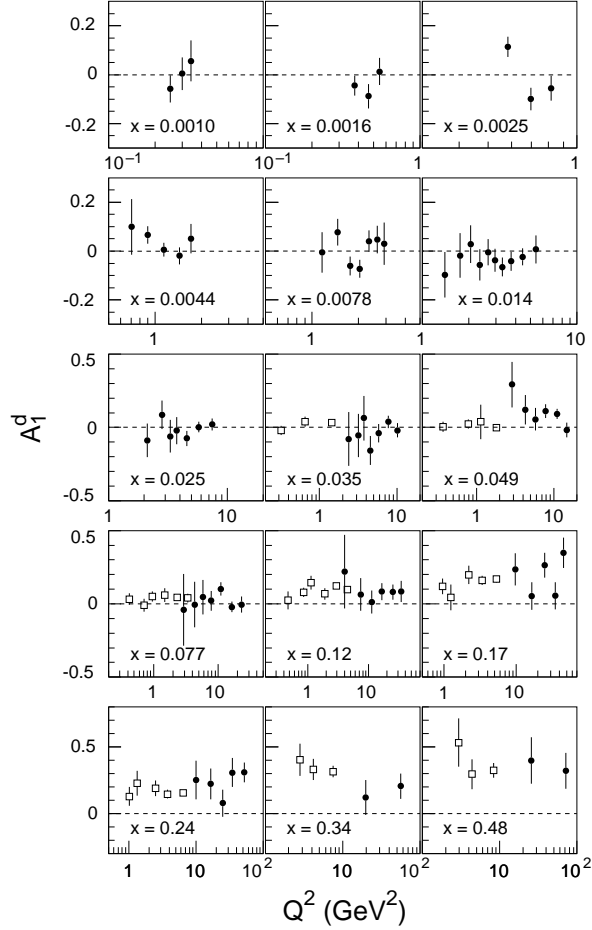


Figure 4: Virtual-photon asymmetry of the deuteron, A_1^d , as a function of Q^2 in several x bins from the SMC⁷ (full circles) and E-143¹⁸ (open squares).

4 Test of the Sum Rules

To evaluate the Ellis–Jaffe³⁵ and Bjorken¹⁵ sum rules for the first moments of g_1 ,

$$\Gamma_1(Q_0^2) = \int_0^1 g_1(x, Q_0^2) dx, \quad (8)$$

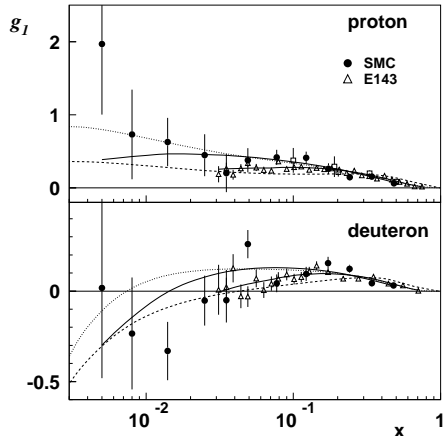


Figure 5: NLO QCD fits⁸ to the SMC and E-143 proton (top) and deuteron data (bottom) for the Q^2 of the measurement (solid line), $Q^2 = 1 \text{ GeV}^2$ (dashed), and $Q^2 = 10 \text{ GeV}^2$ (dotted).

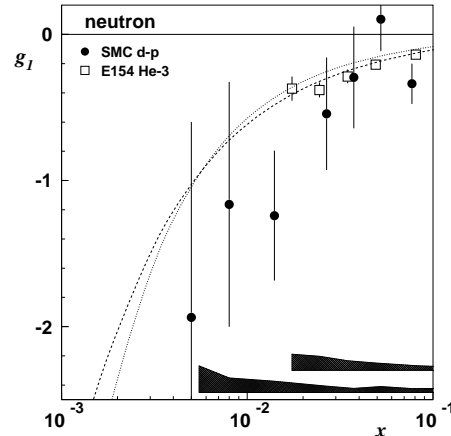


Figure 6: The structure function g_1 of the neutron as a function of x in the small- x region. Also shown are the QCD fits for $Q^2 = 1 \text{ GeV}^2$ (dashed line) and 10 GeV^2 (dotted line). The E-154 data are preliminary.

the structure functions have to be known at a fixed, preferably high, value Q_0^2 of Q^2 . Experiments cannot presently provide this kind of data because Q^2 is limited by the incident lepton energy, E , to $Q^2 \leq 2ME_x$. Thus at small x the data necessarily are obtained at small Q^2 . Until recently the standard procedure to evaluate Γ_1 from the asymmetries was to assume scaling of either A_1 or of $g_1/F_1 \simeq A_1$ and thus to account only for the Q^2 evolution of F_2 and R in Eq. 6.

The second potentially dangerous step in the evaluation of Γ_1 is the extrapolation from the measured region to $x = 0$, i.e. from $x \geq 0.03$ for the SLAC and $x \geq 0.003$ for the SMC data. This extrapolation is usually performed assuming a Regge-type behaviour³⁶ of the form $g_1 \propto x^{-\alpha}$ with $-0.5 < \alpha < 0$.³⁷ However, the theoretically proposed shapes vary widely^{38,39} and the onset of a certain predicted behaviour is usually not well defined. Therefore it is mandatory to measure to as small values of x as possible. In perturbative QCD one expects⁴⁰ that g_1 turns negative at small x and reasonably high Q^2 . Such a drop is visible in the SMC neutron data and was recently confirmed by the preliminary E-154 neutron data¹³ for the region, $x > 0.014$ (Fig. 6). This x behaviour is incompatible with the Regge-like behaviour of g_1^p for $x < 0.03$ assumed in the analysis of the earlier E-142 data. As is obvious from Fig. 6 it

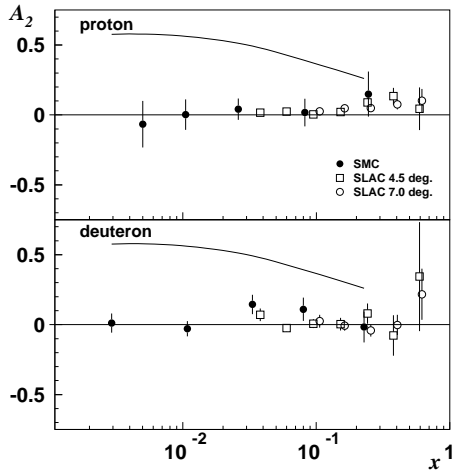


Figure 7: The asymmetry A_2 as a function of x for the proton and the deuteron from the SMC and SLAC E-143 experiments.^{8, 7, 12} Also shown is the limit \sqrt{R} for the kinematics of the SMC experiments (solid line).

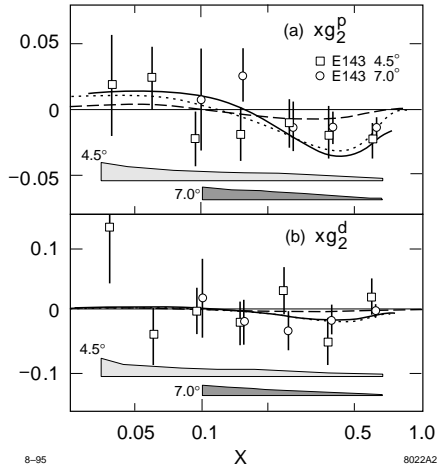


Figure 8: The structure function g_2 as a function of x for the proton and the deuteron from the E-143 experiment.¹² The solid line indicates the twist-2 part g_2^{ww} . The dashed³³ and dotted³⁴ lines refer to bag-model calculations of g_2 .

is difficult to perform a sensible extrapolation to $x = 0$ from the E-154 neutron data alone. The Collaboration only quotes the integral for the measured region, $0.014 < x < 0.7$, of -0.037 ± 0.011 at $Q^2 = 5 \text{ GeV}^2$. Assuming a power law the E-154 Collaboration found¹³ $g_1^n(x \rightarrow 0) = -0.02x^{-0.8}$ corresponding to an integral of -0.043 for $0 \leq x < 0.014$, which would even exceed the contribution from the measured region.

The extrapolation to $x = 1$ is uncritical due to the bound $|A_1| \leq 1$ and the smallness of F_2 in this region. The results for the first moments of g_1 are summarised in Table 2 and are shown in Fig. 9.

The SMC was the first experimental group to include a full next-to-leading order QCD evolution in their analyses^{8, 7} (Figs. 5, 6). The effect of the evolution from the Q^2 of the measurement, Q_m^2 , to Q_0^2 was estimated by

$$g_1(x, Q_0^2) = g_1(x, Q_m^2) + \{g_1^{\text{fit}}(x, Q_0^2) - g_1^{\text{fit}}(x, Q_m^2)\}, \quad (9)$$

where g_1^{fit} refers to g_1 as calculated from the fitted parton distribution functions. The differences of the first moments obtained with QCD evolution and with the scaling assumption for A_1 are small (Table 2), partly due to cancellations of contributions from different x regions. The Ellis-Jaffe pre-

Table 2: Results for the Ellis–Jaffe sum, $\Gamma_1(Q_0^2)$

	$\langle Q_0^2 \rangle$	Proton	Deuteron	Neutron	Bjorken
SMC	10	0.136 (16)	0.041 (7)	<i>-0.047 (21)</i>	0.183 (34)
SMC ^{scale}	10	0.139 (17)	0.037 (8)	<i>-0.059 (24)</i>	0.198 (35)
E-143	3	0.127 (11)	0.042 (5)	<i>-0.037 (14)</i>	0.163 (19)
E-142	2			-0.031 (11)	
HERMES	2.5			-0.037 (15)	
SMC ^{comb}	5	0.142 (11)	0.038 (6)	-0.061 (16)	0.202 (22)
ABFR	3	0.114	0.027	-0.056	0.170
Sum	10	0.171 (4)	0.071 (4)	-0.017 (4)	0.187 (2)
rules	5	0.165 (4)	0.071 (4)	-0.016 (4)	0.181 (3)
	3	0.166 (5)	0.070 (4)	-0.015 (4)	0.176 (4)

The SMC and the ABFR³⁰ (Fit A) analyses use NLO QCD evolution. In the SMC^{scale} and the other analyses scaling of A_1 or g_1/F_1 is assumed. The SMC^{comb} analysis includes SMC, E-143, and E-142 data.⁸ The neutron values in *italics* are obtained by combining proton and deuteron data. Statistical and systematic errors were added in quadrature.

dictions given in Table 2 and shown as shaded bands in Fig. 9 were calculated using QCD corrections⁴¹ up to order $\mathcal{O}(\alpha_s^2)$ with three quark flavours, $\alpha_s(M_Z^2) = 0.118 \pm 0.003$,⁴² $g_a = 1.2601 \pm 0.0025$,⁴² and $F/D = 0.575 \pm 0.016$.⁴³ All experiments find a violation of the Ellis–Jaffe sum rule independent of the target material. The most significant results are obtained for the deuteron, where the violation amounts to 4.5 (3.7) standard deviations for the E-143 (SMC) data. Also the re-analysed E-142 neutron data⁹ now show a violation of the sum rule, while when first published⁴⁴ in 1993 agreement was reported.

The results for the Bjorken sum, $\Gamma_1^p - \Gamma_1^n$, are summarised in Table 2 and Fig. 10, where for comparison all experimental results were evolved to $Q^2 = \infty$ using corrections⁴⁵ up to order $\mathcal{O}(\alpha_s^3)$ and the constants given above. All results are in agreement with the Bjorken sum rule prediction, 0.2100 ± 0.0003 , for $Q^2 = \infty$. The value for the E-143 data assuming scaling of A_1 instead of g_1/F_1 was taken from Ref. 46. For the SLAC data obtained at $Q^2 = 3 \text{ GeV}^2$ the agreement improves when higher-order corrections are estimated using the technique of Padé approximants.⁴⁷ For small Q^2 this method yields a much stronger dependence of the Bjorken sum rule on α_s than obtained from the corrections up to $\mathcal{O}(\alpha_s^3)$. As a consequence the determination⁴⁷ of α_s from the Bjorken sum data at small Q^2 results in a very small statistical error, $\alpha_s(M_Z^2) = 0.117^{+0.004}_{-0.007} \pm 0.002$. This method would yield similarly small errors when applied to e.g. the CCFR data⁴⁸ for the Gross–Llewellyn Smith sum.

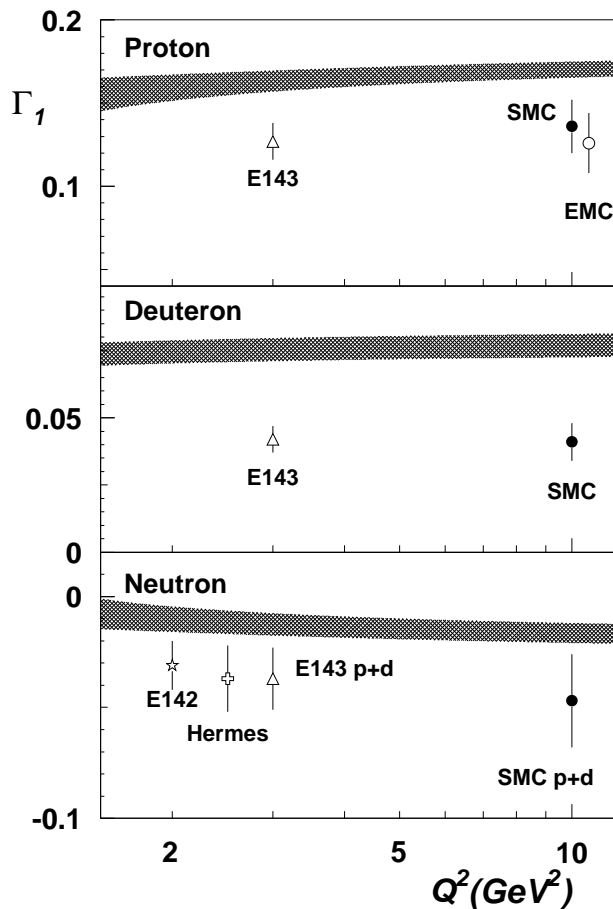


Figure 9: Results for the Ellis–Jaffe sum as a function of Q^2 . The shaded bands indicate the theoretical prediction and its uncertainty.

The assessment of the theoretical uncertainties shown as second error for α_s has been criticised.⁴⁹ Using corrections to $\mathcal{O}(\alpha_s^3)$ only, one obtains³⁰ about three-times larger uncertainties for the strong coupling constant. In this case a more significant result can be obtained³⁰ from the scaling violations of g_1 , $\alpha_s(M_Z^2) = 0.120^{+0.010}_{-0.008}$.

The SMC performed a combined analysis⁸ of the first moments at $Q^2 = 5 \text{ GeV}^2$ using a next-to-leading order QCD evolution. The analysis was performed x bin per x bin and includes all published proton, deuteron, and neutron

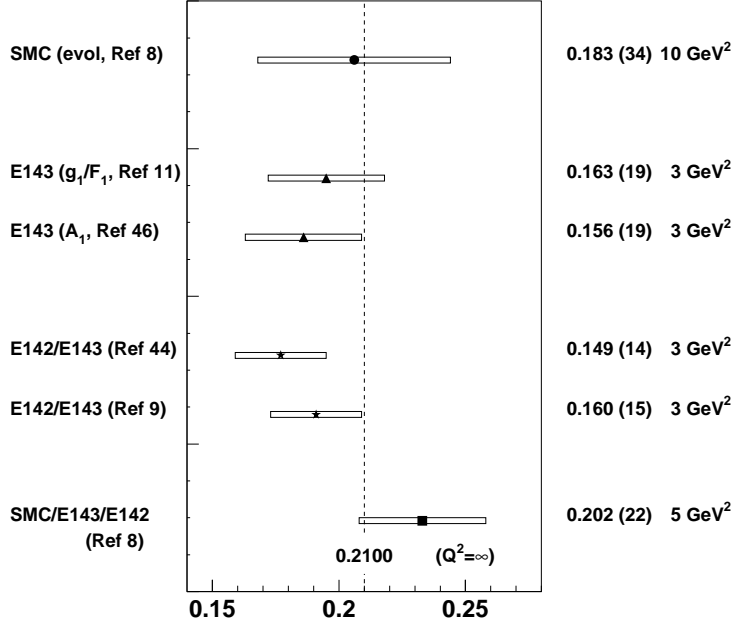


Figure 10: Results for the Bjorken sum for comparison evolved to $Q^2 = \infty$.

data. In such a procedure the SLAC extrapolations for $0.003 < x < 0.03$ are replaced by the SMC small- x data. The result,

$$\Gamma^P - \Gamma^n = 0.202 \pm 0.022 \quad \text{at } Q^2 = 5 \text{ GeV}^2, \quad (10)$$

lies somewhat above the theoretical prediction of 0.181 ± 0.003 . The combined result is larger than the individual results because the SMC data yield a larger contribution at small x than the SLAC extrapolations, while at large x the SLAC data lie slightly above the SMC data. In better agreement with the Bjorken sum rule is the integral of the fitted structure functions from the QCD analysis, which were used to evolve the data, $\int (g_1^p - g_1^n)^{\text{fit}} dx = 0.188$ at $Q^2 = 5 \text{ GeV}^2$. However, this result depends on the parametrisation of the parton distribution functions, particularly in the unmeasured region. In a similar fit³⁰ including also the neutron data the authors of the evolution code found a Bjorken integral of 0.170 at $Q^2 = 3 \text{ GeV}^2$ (Fit A) also in good agreement with the Bjorken sum rule. A significant difference between the two methods is that the SMC combined analysis involves a Regge-type extrapolation, while in the integration method the fitted g_1 is also used in the region $x < 0.003$.

Table 3: Results for $\Delta\Sigma$ and Δs at $Q^2 = \infty$

Exp.	target	$\Delta\Sigma$	Δs
SMC	p	0.25 (15)	-0.11 (5)
SMC	d	0.28 (7)	-0.10 (2)
E-143	p	0.22 (10)	-0.12 (3)
E-143	d	0.30 (5)	-0.09 (2)
E-142	n	0.41 (13)	-0.06 (4)
SMC ^{comb}		0.28 (6)	-0.11 (2)
ABFR		0.10 (7)	

The results for the flavour-singlet axial-current matrix element^b, $\Delta\Sigma$, and the polarisation of the strange quarks, $\Delta s = \int \Delta s(x) dx$, are summarised in Table 3. The values were obtained from the results for Γ_1 using the constants given above. The dependence of $\Delta\Sigma$ on the SU(3) flavour symmetry assumed in the derivation of the Ellis–Jaffe sum rule is weak,⁵⁰ while the result for Δs strongly depends on it. All results are given for $Q^2 = \infty$. The SMC combined result,

$$\Delta\Sigma = 0.28 \pm 0.06 \quad \text{and} \quad \Delta s = -0.11 \pm 0.002, \quad (11)$$

was evaluated in the same way as the combined value for the Bjorken sum and includes the SMC, E-142, and E-143 data. For the polarisation of the up and down quarks the SMC combined analysis yields $\Delta u = 0.81 \pm 0.02$ and $\Delta d = -0.42 \pm 0.02$. A much smaller value for $\Delta\Sigma$ is obtained from QCD fits to the data, due to the different treatment of the unmeasured small x region. For the most significant case, the deuteron, the extrapolation from $x = 0.003$ to $x = 0$ amounts to -0.016 for the fit (ABFR³⁰ in Table 3) at $Q_0^2 = 10 \text{ GeV}^2$, while a Regge-like extrapolation from the SMC deuteron data yields zero. The question of the small- x behaviour of g_1 must eventually be settled by a measurement.

5 Semi-inclusive Asymmetries

In unpolarised deep inelastic scattering the flavour separation of the parton distribution functions is accomplished by the combination of data from charged-lepton and charged-current neutrino scattering, which weight the individual quark flavours differently. Neutrino experiments require huge targets, which

^bNote that the notation $\Delta\Sigma$ corresponds to $a_0(\infty)$ in e.g. Refs. [30, 8].

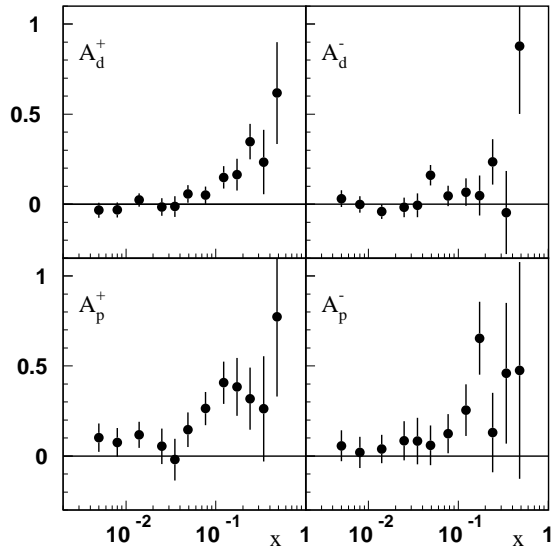


Figure 11: The asymmetries for positive (left) and negative(right) hadrons for deuteron (top) and proton (bottom) targets as a function of x .

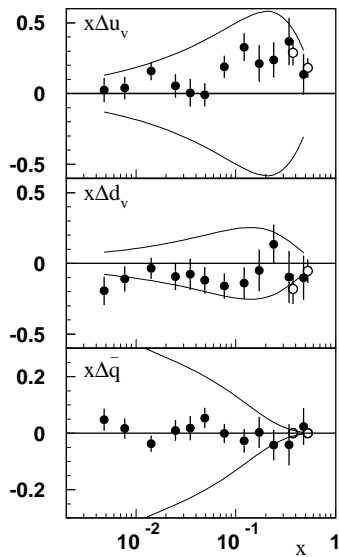


Figure 12: Preliminary SMC data for the polarisation of the valence up and down quarks and the light antiquarks.

are not available in the polarised case. If the HERA proton beam can be polarised, charged-current electron-proton scattering at high Q^2 would become possible.⁵¹ Presently the only access to flavour separation is semi-inclusive scattering, where the emerging hadron carries some memory of the flavour of the initially hit quark. The fragmentation of a quark q into a hadron h is described by the fragmentation functions D_q^h . The fragmentation factorises from the hard scattering process and the differential cross section reads,

$$\frac{1}{\sigma^\mu} \frac{d\sigma^\pm}{dz} = \frac{1}{N^\mu} \frac{dN^\pm}{dz} = \frac{\sum_q e_q^2 q(x, Q^2) D_q^{h^\pm}(z, Q^2)}{\sum_q e_q^2 q(x, Q^2)}, \quad (12)$$

where N^\pm is the number of produced hadrons, N^μ the is the number of deep-inelastic events, $z = E_h/\nu$ is the quark's energy fraction carried by the hadron, and σ^\pm and σ^μ are the inclusive and semi-inclusive differential cross sections. The sums run over $q = u, d, s, \bar{u}, \bar{d}, \bar{s}$ and e_q are the quark charges.

The only data on flavour separation⁶ to date come from the SMC. The preliminary data presented here include the 1995 data set. The asymmetries for positive and negative hadrons for both, proton and deuteron targets, are shown

is Fig. 11. In the analysis a cut of $z > 0.2$ was applied and the fragmentation functions were taken from EMC measurements.⁵² The HERMES Collaboration also presented⁵³ hadron asymmetries for a ^3He target. However, only together with their not yet available 1996 proton data a flavour separation can be performed. The preliminary SMC results for the valence quark distributions, Δq_v with $q_v(x) = q(x) - \bar{q}(x)$, are shown in Fig. 12. The up valence quarks show a positive polarisation over the whole x range, while the down valence quarks are polarised oppositely to the proton spin. For the first moments the SMC obtains $\Delta u_v = 0.85 \pm 0.14 \pm 0.12$, $\Delta d_v = -0.58 \pm 0.16 \pm 0.11$, and $\Delta \bar{q} = 0.02 \pm 0.06 \pm 0.03$, where $\Delta \bar{u}(x) = \Delta \bar{d}(x) := \Delta \bar{q}(x)$ was assumed. The analysis is largely insensitive to $\Delta s(x)$, which was assumed to be proportional to $s(x)$ with a first moment as obtained from Γ_1 .

6 Conclusions and Outlook

The main goals of the experiments initiated after the discovery of the ‘‘EMC spin effect’’, in particular the confirmation of the EMC proton result, the extension of the measurements to smaller x , a measurement of the neutron or deuteron structure function and thus a test of the Bjorken sum rule are now largely achieved. The data from all experiments are in good agreement and draw a consistent picture, where the Bjorken sum rule is tested with a precision of about 10 % and where $\Delta\Sigma$ is of the order of 30 %. However, still the original question raised by the EMC result of how the spin of the nucleon is built up from the spins and the orbital angular momenta of quarks and gluons is unanswered. The interest has now turned to the Q^2 dependence of g_1 and the rôle of the gluon polarisation, Δg , which via the axial anomaly^{54,55,56} contributes to $\Delta\Sigma$. If the violation of the Ellis–Jaffe sum rules is entirely attributed to the anomalous contribution of Δg to $\Delta\Sigma$, a gluon polarisation of $\Delta g = 2.5$ at $Q^2 = 10 \text{ GeV}^2$ is required. QCD analyses indicate that Δg is positive and of about this size.^{30,28} Also a QCD sum rule calculation⁵⁷ indicates a large and positive value for Δg .

To make further progress in our understanding of the nucleon’s spin structure a direct measurement of Δg is indispensable. An unambiguous determination of Δg can only be achieved studying a process where Δg enters in leading order. The cleanest such process is the photon-gluon fusion, which can either be tagged by open charm, $\gamma^*g \rightarrow c\bar{c}$, or 2+1-jet production.⁵⁸ The former is proposed for the approved COMPASS experiment at CERN^{59,60} while the later is aimed at by the project to polarise the HERA proton beam.⁶¹ Processes using hadronic probes, like $p\bar{p}$ collisions at RHIC⁶² are in general more difficult to interpret. A detailed understanding of the nucleon’s spin structure

must also include the third twist-2 structure function, the transversity⁶³ h_1 , which will be studied at HERMES, COMPASS, and RHIC.

Acknowledgements

I like to thank H. Castilla for the inspiring atmosphere in Mexico City, C. W. de Jager, T. J. Ketel, P. J. Mulders, and J. Oberski for their hospitality in Amsterdam, and my colleagues in the SMC for the many discussions which were essential in preparing these talks.

References

- [1] The EM Collaboration, J. Ashman *et al.*, *Phys. Lett. B* **206**, 364 (1988).
- [2] The EM Collaboration, J. Ashman *et al.*, *Nucl. Phys. B* **328**, 1 (1989).
- [3] The SM Collaboration, D. Adams *et al.*, *Phys. Lett. B* **329**, 399 (1994);
erratum Phys. Lett. B **339**, 332 (1994).
- [4] The SM Collaboration, D. Adams *et al.*, *Phys. Lett. B* **336**, 125 (1994).
- [5] The SM Collaboration, D. Adams *et al.*, *Phys. Lett. B* **357**, 248 (1995).
- [6] The SM Collaboration, B. Adeva *et al.*, *Phys. Lett. B* **369**, 93 (1996).
- [7] The SM Collaboration, B. Adeva *et al.*, *Phys. Lett. B* **396**, 338 (1997).
- [8] The SM Collaboration, D. Adams *et al.*, submitted to *Phys. Rev. D*,
hep-ex/9702005.
- [9] The E-142 Collaboration, P. L. Anthony *et al.*, *Phys. Rev. D* **54**, 6620 (1996).
- [10] The E-143 Collaboration, K. Abe *et al.*, *Phys. Rev. Lett.* **74**, 346 (1995).
- [11] The E-143 Collaboration, K. Abe *et al.*, *Phys. Rev. Lett.* **75**, 25 (1995).
- [12] The E-143 Collaboration, K. Abe *et al.*, *Phys. Rev. Lett.* **76**, 587 (1996).
- [13] The E-154 Collaboration, E. Hughes *et al.*, in: *Proceedings Int. Conf. of High Energy Physics*, Warsaw, Poland, July 25, 1996.
- [14] The HERMES Collaboration, K. Ackerstaff *et al.*, Preprint OAP-741 (March 1997), hep-ex/9703005.
- [15] J. D. Bjorken, *Phys. Rev.* **148**, 1467 (1966); *Phys. Rev. D* **1**, 1376 (1970).
- [16] X. Ji, J. Tang, and P. Hoodbhoy, *Phys. Rev. Lett.* **76**, 740 (1996).
- [17] N. W. Schellingerhout *et al.*, *Phys. Rev. C* **48**, 2714 (1993).
- [18] The E-143 Collaboration, K. Abe *et al.*, *Phys. Lett. B* **364**, 61 (1995).
- [19] The NM Collaboration, P. Amaudruz *et al.*, *Phys. Lett. B* **295**, 159 (1992).
- [20] The NM Collaboration, M. Arneodo *et al.*, *Phys. Lett. B* **364**, 107 (1995).
- [21] L. W. Whitlow *et al.*, *Phys. Lett. B* **250**, 193 (1990).
- [22] The NM Collaboration, M. Arneodo *et al.*, *Nucl. Phys. B* **483**, 3 (1997).
- [23] G. Altarelli and G. Martinelli, *Phys. Lett. B* **76**, 89 (1978).
- [24] G. K. Mallot, in: B. Frois, N. de Groot, and V. W. Hughes, *Proceedings Ettore Majorana International School of Nucleon Structure: 1st Course: The Spin Structure of the Nucleon*, Erice, Italy, 3–10 Aug 1995, (World Scientific, Singapore), to be published, hep-ex/9703014.

- [25] R. Mertig and W. L. van Neerven, *Z. Phys. C* **70**, 637 (1996).
- [26] W. Vogelsang, *Phys. Rev. D* **54**, 2023 (1996).
- [27] T. Gehrmann and W. J. Stirling, *Phys. Rev. D* **53**, 6100 (1996).
- [28] M. Glück, E. Reya, M. Stratmann, and W. Vogelsang, *Phys. Rev. D* **53**, 4775 (1996).
- [29] R. D. Ball, S. Forte, and G. Ridolfi, *Phys. Lett. B* **378**, 255 (1996).
- [30] G. Altarelli, R. D. Ball, S. Forte, and G. Ridolfi, Preprint CERN-TH-96-345 (Geneva, Dec. 1996), hep-ph/9701289
- [31] S. Wandzura and F. Wilczek, *Phys. Lett. B* **72**, 195 (1977).
- [32] R. L. Jaffe, *Comments Nucl. Part. Phys.* **19**, 239 (1990).
- [33] X. Song and J. S. McCarthy, *Phys. Rev. D* **49**, 3169 (1994), *erratum ibid.* **50**, 4718 (1994).
- [34] M. Stratmann, *Z. Phys. C* **60**, 763 (1993).
- [35] J. Ellis and R. L. Jaffe, *Phys. Rev. D* **9**, 1444 (1974); *Phys. Rev. D* **10**, 1669 (1974).
- [36] R. L. Heimann, *Nucl. Phys. B* **64**, 429 (1973).
- [37] J. Ellis and M. Karliner, *Phys. Lett. B* **213**, 73 (1988).
- [38] S. D. Bass and P. V. Landshoff, *Phys. Lett. B* **336**, 537 (1994).
- [39] F. E. Close and R. G. Roberts, *Phys. Lett. B* **336**, 257 (1994).
- [40] R. D. Ball, S. Forte, and G. Ridolfi, *Nucl. Phys. B* **444**, 287 (1995), *erratum Nucl. Phys. B* **449**, 680 (1995).
- [41] S. A. Larin, *Phys. Lett. B* **334**, 192 (1994).
- [42] The Particle Data Group, R. M. Barnett *et al.*, *Phys. Rev. D* **50**, 1 (1994).
- [43] F. E. Close and R. G. Roberts, *Phys. Lett. B* **316**, 165 (1993).
- [44] The E-142 Collaboration, D. L. Anthony *et al.*, *Phys. Rev. Lett.* **71**, 959 (1993).
- [45] S. A. Larin and J. A. M. Vermaseren, *Phys. Lett. B* **259**, 345 (1991).
- [46] J. McCarthy, O. A. Rondon, and T. J. Liu, *Phys. Rev. D* **54**, 2391 (1996).
- [47] J. Ellis, E. Gardi, M. Karliner, and M. A. Samuel, *Phys. Lett. B* **366**, 268 (1996).
- [48] The CCFR Collaboration, D. A. Harris *et al.*, in: J. Tran Thanh Van, ed., *Proceedings XXXth Rencontres de Moriond: QCD and High Energy Hadronic Interactions*, Meribel les Allues, France, 19–25 Mar 1995, (Editions Frontières, France, 1995) 247, hep-ex/9506010.
- [49] S. Forte, in: *Proceedings 12th International Symposium on High-Energy Spin Physics (SPIN 96)*, Amsterdam, The Netherlands, 10–14 Sep 1996, hep-ex/9610238.
- [50] J. Lichtenstadt and H. J. Lipkin, *Phys. Lett. B* **353**, 119 (1995).
- [51] M. Anselmino, P. Gambino, and J. Kalinowski, to be published in *Phys. Rev. D*, hep-ph/9607427.
- [52] The EM Collaboration, M. Arneodo *et al.*, *Nucl. Phys. B* **321**, 541 (1989).
- [53] The HERMES Collaboration, E. E. W. Bruins *et al.*, in: *Proceedings 12th International Symposium on High-Energy Spin Physics (SPIN 96)*, Amsterdam, The Netherlands, 10–14 Sep 1996, hep-ex/9611010.

- [54] A. V. Efremov and O. V. Teryaev, Preprint E2-88-287 (Dubna, Russia, 1988), in: J. Fischer *et al.*, eds., Proceedings *Int. Hadron Symposium*, Bechyne, Czechoslovakia, 1988, (Czech. Academy of Science, Prague, 1989) 302.
- [55] G. Altarelli and G. G. Ross, *Phys. Lett. B* **212**, 391 (1988).
- [56] R. D. Carlitz, J. C. Collins, and A. H. Mueller, *Phys. Lett. B* **214**, 229 (1988).
- [57] L. Mankiewicz, G. Piller, and A. Saalfeld, Preprint TUM-T39-96-26 (TU Munich, Germany, November 1996), hep-ph/9611326.
- [58] The H1 Collaboration, S. Aid *et al.*, *Nucl. Phys. B* **449**, 3 (1995).
- [59] The COMPASS Collaboration, COMPASS proposal, CERN/SPSLC 96-14, SPSC/P297 (Geneva, March 1996); CERN/SPSLC 96-30 (Geneva, May 1996).
- [60] G. K. Mallot, in: Proceedings *12th International Symposium on High-Energy Spin Physics (SPIN 96)*, Amsterdam, The Netherlands, 10–14 Sep 1996, hep-ex/9611016.
- [61] G. Ingelman, A. De Roeck, and R. Klanner, eds., Proceedings *Future Physics at HERA*, (Hamburg, Germany, September 1996), <http://www.desy.de/~heraws96>.
- [62] The RHIC Spin Collaboration, M. Beddo *et al.*, Proposal on Spin Physics Using the RHIC polarized Collider, (BNL, Upton, NY, August, 1992).
- [63] R. L. Jaffe and X. Ji, *Nucl. Phys. B* **375**, 527 (1992).